Supporting Information

Regiochemical memory in the adiabatic photolysis of thymine-derived oxetanes. A combined ultrafast spectroscopic and CASSCF/CASPT2 computational study

Alejandro Blasco-Brusola, Miriam Navarrete-Miguel, Angelo Giussani, Daniel Roca-Sanjuán,* Ignacio Vayá,* Miguel A. Miranda*

Table of contents

Fig. S5 Natural orbitals of the CASSCF active space of the singlet states at the exciplex structure for HH-1. π_{DMT}* and $\pi_{C,BP}$* can be considered the σ and σ* orbitals of the C-C and C-O bonds that break throughout the process.

Fig. S6 Natural orbitals of the CASSCF active space of the triplet states at the exciplex structure (^{3}[BP···DMT]*) for HH-1. $\pi_{BP(DMT)}$* and $\pi_{DMT(BP)}$* can be considered the σ and σ* orbitals of the C-C and C-O bonds that break throughout the process.

Fig. S7 Natural orbitals of the CASSCF active space of the singlet states at the oxetane structure (OXE) for HT-1.

Fig. S8 Natural orbitals of the CASSCF active space of the singlet states of at the diradical structure (^{1}DIR*) for HT-1. $\pi_{C,DMT}$ and $\pi_{C,BP}$ can be considered the σ and σ* orbitals of the C-C bond that breaks throughout the process.

Fig. S9 Natural orbitals of the CASSCF active space of the triplet states at the diradical structure (^{3}DIR*) for HT-1.

Fig. S10 Natural orbitals of the CASSCF active space of the singlet states at the exciplex structure for HT-1. $\pi_{BP(DMT)}$* and $\pi_{DMT(BP)}$* can be considered the σ and σ* orbitals of the C-C and C-O bonds that break throughout the process.

Fig. S11 Natural orbitals of the CASSCF active space of the triplet states at the exciplex structure (^{3}[BP···DMT]*) for HT-1. $\pi_{DMT(BP)}$* and $\pi_{BP(DMT)}$* can be considered the σ and σ* orbitals of the C-C and C-O bonds that break throughout the process.

Fig. S12 Natural orbitals of the CASSCF active space at the equilibrium structure of the S_1 state at the diradical region (^{1}DIR*) for HH-1. $\pi_{BP(DMT)}$ and $\pi_{BP(DMT)}$* can be considered the σ and σ* orbitals of the C-C bond that breaks throughout the process.

Fig. S13 Natural orbitals of the CASSCF active space at the equilibrium structure of the S_1 state at the diradical region (^{1}DIR*) for HT-1. $\pi_{C,DMT}$ and $\pi_{C,BP}$* can be considered the σ and σ* orbitals of the C-C bond that breaks throughout the process.

Fig. S14 Femtosecond transient absorption spectra from 0.1 to 40 ps for (A) BP, (B), HH-1 and (C) HT-1 after excitation at 280 nm in MeCN.

Materials and methods

Chemicals and Reagents

Benzophenone and thymine were purchased from Sigma-Aldrich. Spectrophotometric HPLC solvents were obtained from Scharlab and used without further purification.

Spectroscopic Techniques

The ^{1}H-NMR spectra were recorded in $CDCl_3$ at 400 MHz using a Bruker AVANCE III instrument; chemical shifts are reported in ppm.

Laser Flash Photolysis (LFP) measurements were performed using a pulsed Nd: YAG L52137 V LOTIS TII at the excitation wavelength of 266 nm or 355 nm. The single pulses were *ca*. 10 ns duration, and the energy was ~12 mJ/pulse. The laser flash photolysis system consisted of the pulsed laser, a 77250 Oriel monochromator and an oscilloscope DP04054 Tektronix. The output signal from the oscilloscope was transferred to a personal computer. Absorbances of HH-1, HT-1 and BP in MeCN were adjusted at ~0.20 at 266 nm. Quenching of the triplet excited state of benzophenone (2 mM) after addition of increasing amounts of DMT were performed at λ_{exc} = 355 nm. All measurements were done using 10 × 10 mm^2 quartz cuvettes at room temperature in deaerated conditions (25 min N_2 bubbling), using 30 mL of fresh solution in order to avoid data acquisition from photodegraded products.

Femtosecond transient absorption experiments were performed using a typical pump-probe system. The femtosecond pulses were generated with a mode-locked Ti-Sapphire laser of a compact Libra HE (4 W power at 4 kHz) regenerative amplifier delivering 100 fs pulses at 800 nm (1 mJ/pulse). The output of the laser was split into two parts to generate the pump and the probe beams. Thus, tunable femtosecond pump pulses were obtained by directing the 800 nm light into an optical parametric amplifier. In the present case, the pump was set at 280 nm and passed through a chopper prior to focus onto a rotating cell (1 mm optical path) containing the samples in organic solution. The white light used as probe was produced after part of the 800 nm light from the amplifier travelled through a computer controlled 8 ns variable optical delay line and impinge on a CaF_2 rotating crystal. This white light was in turn split in two identical portions to generate reference and probe beams that then are focused on the rotating cell containing the sample. The pump and the probe beams were made to coincide to interrogate the sample. The power of the pump beam was set to 180 μW. A computer-controlled imaging spectrometer was placed after this path to measure the probe and the reference pulses to obtain the transient absorption decays/spectra. The experimental data were treated and compensated by the chirp using the ExciPro program.

Computational Details

Density functional theory (DFT) and multiconfigurational quantum chemistry (CASSCF and CASPT2) was used for the computations of this work by using the GAUSSIAN 09, revision D.01,[1] and MOLCAS 8[2] software packages, respectively.

Geometry optimizations. The structures of the singlet ground state of the oxetane (OXE), the triplet state of the diradical (^{3}DIR*), the triplet state of the exciplex (^{3}[BP···DMT]*), the triplet transition state (TS) between the diradical and the exciplex

and the isolated BP and DMT molecules were optimized using the DFT method with the M06-2X functional, without any symmetry restriction and the standard 6-31++G** basis set. The equilibrium structure of the S_1 state of the diradical (^{1}DIR*) was determined with the CASSCF method, with an active space of 6 electrons distributed in 6 orbitals, and the atomic natural orbital (ANO) S-type valence double-ζ plus polarization (ANO-S-VDZP) basis set.

On the one hand, a series of intermediate geometries were obtained by means of the linear interpolation of internal coordinates (LIIC) technique between OXE, ^{3}DIR*, TS and ^{3}[BP···DMT]* of HH-1. This strategy provides connected but non-optimized paths, therefore, the energy barriers must be considered as upper bounds. For HT-1, LIIC procedure was also used to obtain geometries between ^{3}DIR*, TS and ^{3}[BP···DMT]*. Meanwhile, between OXE and ^{3}DIR*, due to invalid interpolated structures obtained in the LIIC procedure, ground-state (S_0) constrained geometries were determined using the C-C bond length as scanning coordinate and with the M06-2X/6-31++G** level of theory.

Excited-state single-point calculations. The ground- and excited-state energies on top of the optimized and LIIC (or scanned) geometries were calculated using the state specific (SS)-CASPT2 method, which includes the dynamic correlation, with the state averaged (SA)-CASSCF wave functions with an active space of 12 electrons distributed in 12 orbitals, demanding three singlet and three triplet states in the SA-CASSCF procedure and with the ANO-S-VDZP basis set. The ionization-potential electron-affinity parameter (IPEA) was set to 0.0 au as originally established in MOLCAS, and an imaginary level shift of 0.2 au^3 was used to minimize the presence of weakly intruder states. Oscillator strengths (*f*) at the exciplex were calculated according to the formula $f = \frac{2}{3} E_{VA} TDM^2$, where E_{VA} stands for the CASPT2 vertical absorption energy, and TDM refers to the transition dipole moment between the initial φ_1 and final φ_2 SA-CASSCF wave functions, according to the formula $TDM = \langle \varphi_1 | \vec{d} | \varphi_2 \rangle$, where $\vec{d}$ is the dipole moment operator.

Binding energies of the triplet exciplex. They were determined by the formula *^{3}BP* + ^{1}DMT* – ^{3}[BP···DMT]**, where the terms stand for the triplet lowest-energy state of the optimized isolated BP, the singlet ground-state energy of the optimized isolated DMT and the triplet lowest-energy state of the optimized exciplex, respectively. Distinct levels of theory were used: (i) DFT/M06-2X/6-31++G** level of theory, (ii) level (i) with the Grimme's dispersion with the original D3 damping function,[4, 5] (iii) level (i) with the polarizable continuum model (PCM) with the default parameters of GAUSSIAN 09, revision D.01, for the MeCN solvent, (iv) CASPT2/ANO-S-VDZP energies on top of DFT geometries obtained at the level (i) and (v) CASPT2/ANO-S-VDZP energies on top of DFT geometries with PCM obtained at the level (iii). For (v) the solvent correction computed at the DFT level in (iii) was used. Basis set superposition error (BSSE) does not affect significantly DFT energies but it does contribute to the CASPT2 energies and therefore it must be corrected. Therefore, for (iv) and (v), the counterpoise (CP) correction[6] was computed as originally described elsewhere.[7]

Benchmarking of methodology and additional theoretical analyses

Choice of the active space for the CASSCF/CASPT2 computations. The choice of the active space (CAS(12,12)) was made based on our previous knowledge of studies of the monomers thymine and BP and dimers of nucleobases.[8-10] For nucleobases, 6 π and π^* orbitals per molecule is an acceptable choice in dimer computations.[9] For BP, the same size is also reasonable for $\pi\pi^*$ states. For $n\pi^*$ states, the oxygen lone pair (n) can be added.[8] To keep an efficient CAS and with the same size for all the structures and both systems in our study, we used CAS(12,12). The $n\pi^*$ state of BP only appears at the ^{3}[BP…DMT]* geometry for the S_1. As shown in our previous study in BP,[8] while T_1 has mainly $\pi\pi^*$ nature, S_1 is $n\pi^*$. CAS(14,13) test computations at the ^{3}[BP…DMT]* structure for HH-1 show that indeed T_1 keeps the same energy and, as expected, S_1 deviates more, increasing its relative energy (Table S6). This state in this region does not affect, however, the general conclusions of the work. Regarding the active orbitals in the singlet and triplet computations of this point (^{3}[BP…DMT]*) for HH-1 and HT-1 (Figures S5, S6, S10 and S11), note also that for the singlets of HH-1, the inclusion of this lone pair converged to a solution in which the σ and σ^* orbitals are present. Attempts made to remove those orbitals from the active space were made, but in this way the lone pair was not included and the solution without the lone pair ($\pi\pi^*$ state) was higher in energy, as was expected since the lowest excited state is $n\pi^*$. This was not happening for HT-1 despite starting from the same guess orbitals and reflects intrinsic differences in the electronic structure of both systems.

State-specific (SS) and multistate (MS) CASPT2. The energy splitting at the ^{3}DIR* was compared at both levels of theory to further analyze the accuracy of the SS-CASPT2 for this region; S_0S_1 gap here is crucial in the comparison between HH-1 and HT-1. As shown in Table S7, MS slightly increases this gap but the with a similar value for HH-1 and HT-1 therefore maintaining the trends and the comparative behavior between both systems. Note that, as pointed out in previous studies, the real solution within the CASPT2 framework can be expected in between the gaps provided at the SS and MS levels.[11]

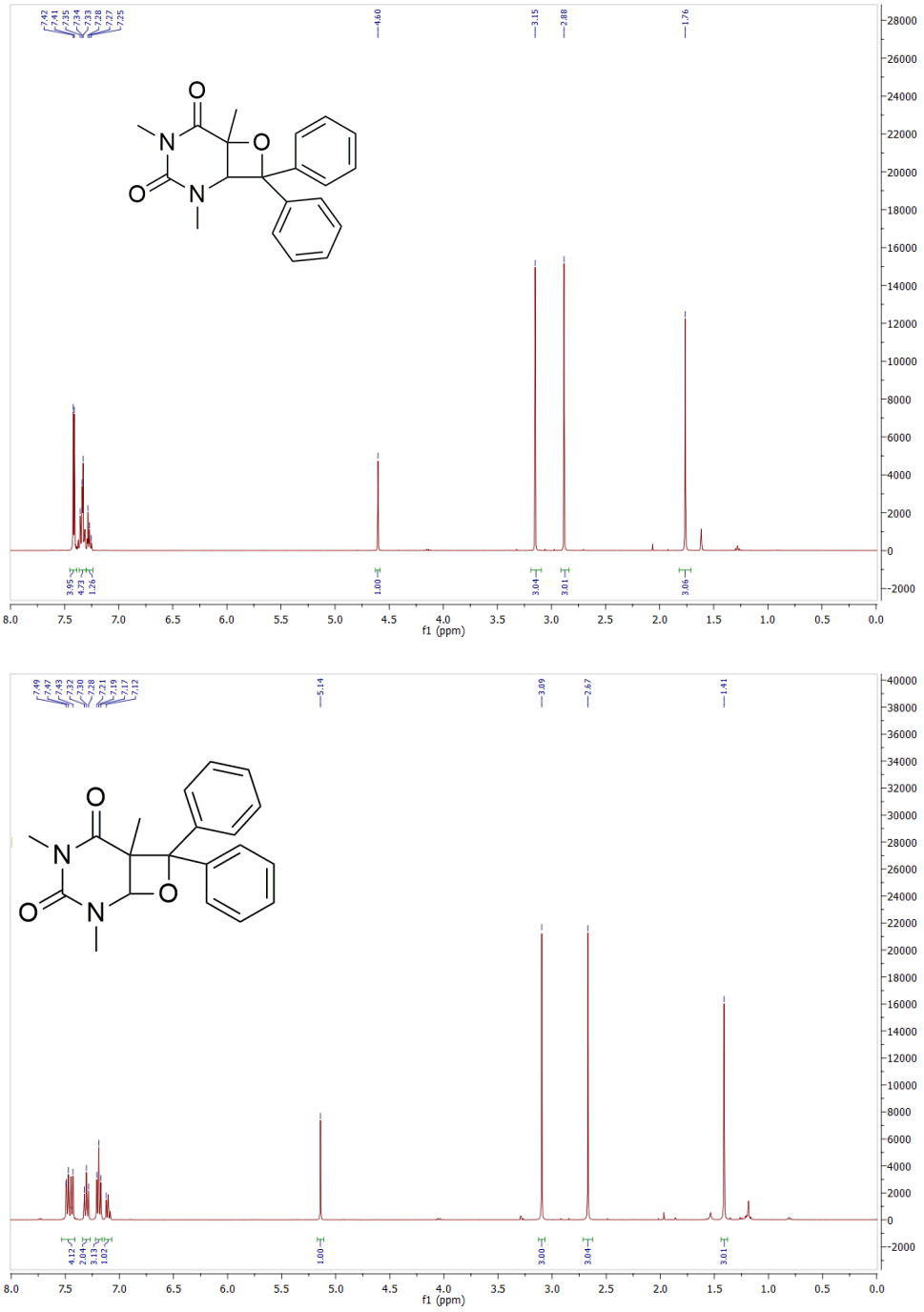

Fig. S1 ^{1}H-NMR spectra of HH-1 (top) and HT-1 (bottom) in $CDCl_3$.

Table S1 Nature of the states in each relevant geometry for HT-1: energies (E; in eV), weight of the main configuration state functions in the CASSCF wavefunction and dipole moment (μ; in Debye). The reference energy is the sum of the separated triplet BP and ground state DMT molecules. See shape of the natural orbitals in Figs. S2-S13.

Geometry	State	Nature	E	Weight	μ
OXE	S_0	cs (HF)[a]	-2.91	0.831	1.93
	S_1	$\pi_{BP1} \rightarrow \pi^*_{BP2}$ $\pi_{BP2} \rightarrow \pi^*_{BP1}$	2.11	0.372 0.314	1.87
^{3}DIR*	S_0	$\pi_{C,DMT} \rightarrow \pi^*_{C,BP}$	-1.19	0.736	2.85
	S_1	cs (HF)[a]	-0.4	0.730	9.94
	T_1	$\sigma_{CC,BP-DMT} \rightarrow \sigma^*_{CC,BP-DMT}$	-0.96	0.798	2.66
^{3}[BP···DMT]*	S_0	cs (HF)[a]	-2.80	0.770	2.58
	S_1	$n_{O,BP} \rightarrow \pi^*_{BP(DMT)}$ $n_{O,BP} \rightarrow \pi^*_{DMT(BP)}$	0.15	0.333 0.207	3.44
	T_1	$\pi_{DMT} \rightarrow \pi^*_{DMT(BP)}$ $\pi_{DMT} \rightarrow \pi^*_{DMT,BP}$	-0.60	0.551 0.280	2.71
^{1}DIR*	S_0	cs (HF)[a]	-1.02	0.925	11.60
	S_1	$\pi_{C,DMT} \rightarrow \pi^*_{C,BP}$	-0.43	0.916	4.35

[a] Closed-shell Hartree-Fock configuration state function.

Table S2 Nature of the states in each relevant geometry for HH-1: energies (E; in eV), weight of the main configuration state functions in the CASSCF wavefunction and dipole moment (μ; in Debye). The reference energy is the sum of the separated triplet BP and ground state DMT molecules. See shape of the natural orbitals in Figs. S2-S13.

Geometry	State	Nature	E	Weight	μ
OXE	S_0	cs (HF)[a]	-2.59	0.860	4.14
	S_1	$\pi_{BP3} \rightarrow \pi^*_{BP1}$ $\pi_{BP1} \rightarrow \pi^*_{BP3}$	2.47	0.391 0.333	4.00
^{3}DIR*	S_0	cs (HF)[a] $2\ (\sigma_{CC} \rightarrow \sigma^*_{CC})$	-0.79	0.418 0.356	4.20
	S_1	$2\sigma_{CC} \rightarrow \pi^*_{BP1}\sigma^*_{CC}$ $\pi_{BP1} \rightarrow \pi^*_{BP1}$ $\sigma_{CC} \rightarrow \pi^*_{BP1}$ $\pi_{BP1}\sigma_{CC} \rightarrow \pi^*_{BP1}\sigma^*_{CC}$	1.57	0.212 0.187 0.124 0.102	4.01
	T_1	$\sigma_{CC} \rightarrow \sigma^*_{CC}$	-0.81	0.796	4.13
^{3}[BP···DMT]*	S_0	cs (HF)[a]	-2.84	0.768	7.87
	S_1	$n_{O,BP} \rightarrow \pi^*_{C,BP}$	-0.34	0.844	4.22
	T_1	$\pi_{DMT} \rightarrow \pi^*_{(BP)DMT}$	-0.53	0.619	6.18
^{1}DIR*	S_0	cs (HF)[a] $\pi_{DMT} \rightarrow \pi^*_{(BP)DMT}$ $\pi_{DMT} \rightarrow \pi^*_{BP1}$ $2\ (\pi_{DMT} \rightarrow \pi^*_{(BP)DMT})$ $\pi_{BP1}\pi_{DMT} \rightarrow \pi^*_{BP1}\pi^*_{(BP)DMT}$	0.56	0.139 0.371 0.118 0.126 0.122	3.68
	S_1	cs (HF)[a] $\pi_{DMT} \rightarrow \pi^*_{BP-DMT}$ $\pi_{BP(DMT)} \rightarrow \pi^*_{BP-DMT}$ $2\ (\pi_{DMT} \rightarrow \pi^*_{BP-DMT})$ $2\pi_{DMT} \rightarrow \pi^*_{BP-DMT}\pi^*_{BP(DMT)}$	0.96	0.195 0.230 0.114 0.176 0.122	3.63

[a] Closed-shell Hartree-Fock configuration state function.

Table S3 Binding energies calculated with different levels of theory (see Computational Details) for both triplet exciplexes (^{3}[BP···DMT]*) of HH-1 and HT-1.

	HH-1 (eV)	HT-1 (eV)	HH-1 (kcal/mol)	HT-1 (kcal/mol)
DFT GD3	0.50	0.60	11.5	13.8
DFT	0.43	0.49	9.9	11.3
DFT PCM	0.40	0.33	9.2	7.6
CASPT2	0.53	0.60	12.2	13.8
CASPT2 PCM	0.50	0.44	11.5	10.1

Table S4 Oscillator strengths and energies of the lowest-energy transitions at the triplet exciplex (^{3}[BP···DMT]*) for HH-1.

Transition	Osc. Strength	Energy (nm)	Energy (eV)
$T_1 \rightarrow T_2$	$2.12 \cdot 10^{-6}$	940	1.32
$T_1 \rightarrow T_3$	$4.13 \cdot 10^{-6}$	841	1.47
$T_1 \rightarrow T_4$	$2.64 \cdot 10^{-7}$	561	2.21
$T_1 \rightarrow T_5$	$1.72 \cdot 10^{-6}$	434	2.86
$T_1 \rightarrow T_6$	$5.75 \cdot 10^{-4}$	377	3.29
$T_1 \rightarrow T_7$	0.014767	378	3.28

Table S5 Nature of the triplet T_1 and T_7 states at the triplet exciplex (^{3}[BP···DMT]*) for HH-1 and weight of the main configuration state functions (CSFs). Single-occupied natural orbitals in each CSF are shown. See shape of the natural orbitals in Fig. S6.

Geometry	State	Nature	Weight
^{3}[BP···DMT]*	T_1	$\pi_{DMT}\pi^*_{DMT(BP)}$	0.625
	T_7	$\pi_{BP2}\pi^*_{DMT(BP)}$	0.201
		$\pi_{BP2}\pi^*_{DMT(BP)}\pi_{DMT}\pi^*_{BP(DMT)}$	0.189
		$\pi_{BP2}\pi^*_{DMT(BP)}\pi_{DMT}\pi^*_{BP(DMT)}$	0.161

Table S6 CASPT2 energy gaps (in eV) at the ^{3}[BP···DMT]*of the HH-1 system calculated with the active spaces CAS(12,12) and CAS (14,13).

	CAS(12,12)	**CAS(14,13)**
S_1S_0	2.503	3.473
T_1S_0	2.307	2.382
T_2S_0	3.705	3.810
T_3S_0	3.773	3.832

Table S7 SS and MS-CASPT2 energy gaps (in eV) between states at the ^{3}DIR* for HH-1 and HT-1.

	HH-1		HT-1	
	ΔE (SS-CASPT2)	**ΔE (MS-CASPT2)**	**ΔE (SS-CASPT2)**	**ΔE (MS-CASPT2)**
S_1S_0	2.357	2.758	0.796	1.204
T_1S_0	-0.027	-0.009	0.232	0.294
T_2T_1	2.442	2.838	2.441	2.836
T_3T_2	0.691	0.735	0.687	0.775

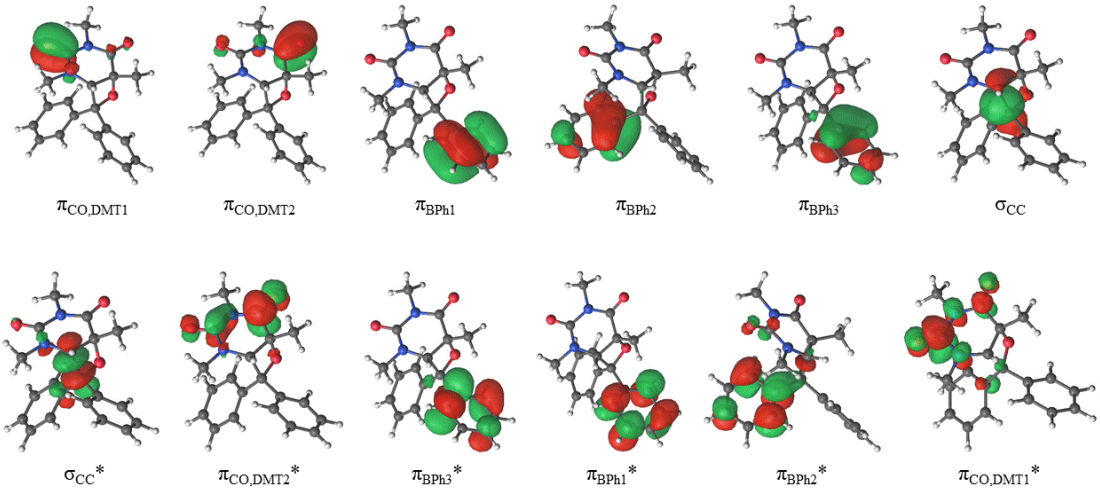

Fig. S2 Natural orbitals of the CASSCF active space of the singlet states at the oxetane structure (OXE) for HH-1.

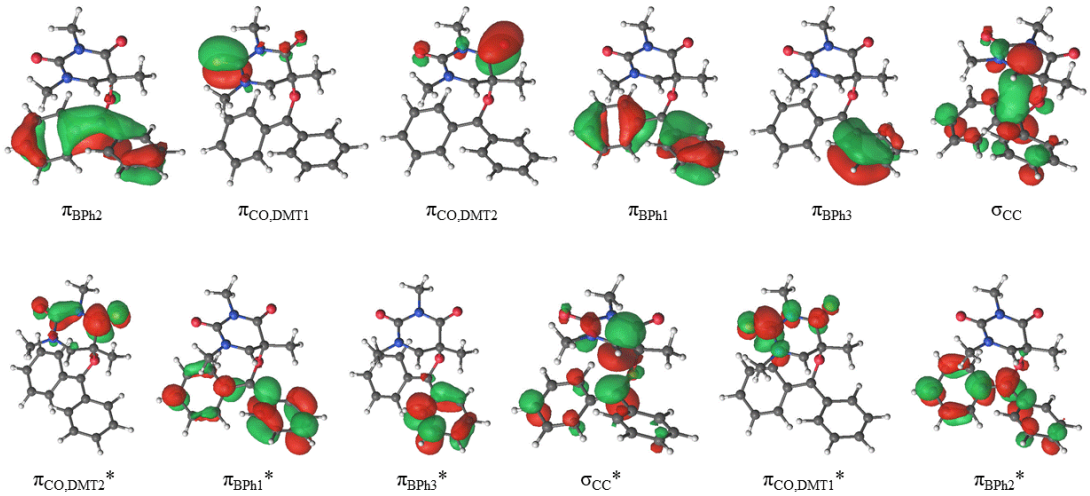

Fig. S3 Natural orbitals of the CASSCF active space of the singlet states at the diradical structure (^{1}DIR*) for HH-1.

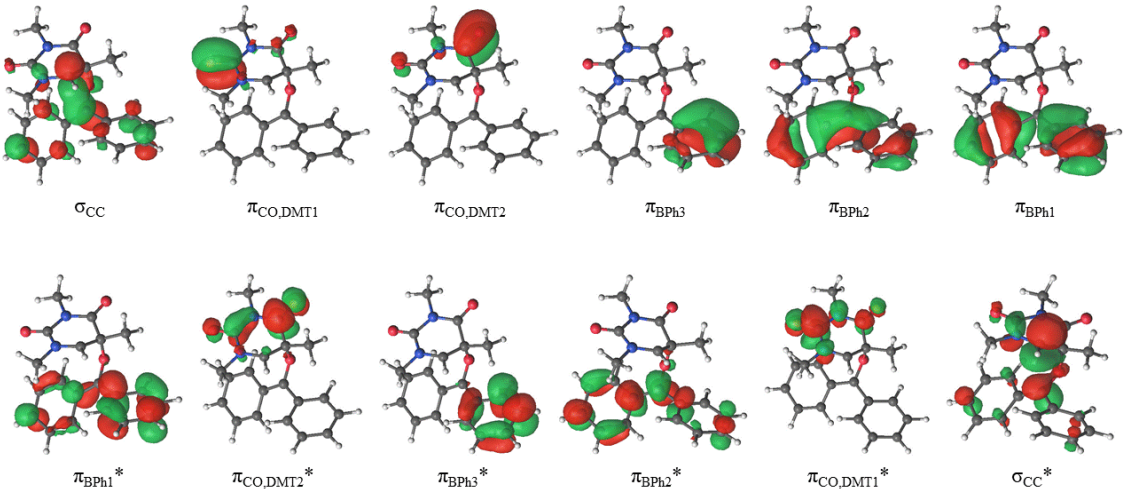

Fig. S4 Natural orbitals of the CASSCF active space of the triplet states at the diradical structure (^{3}DIR*) for HH-1.

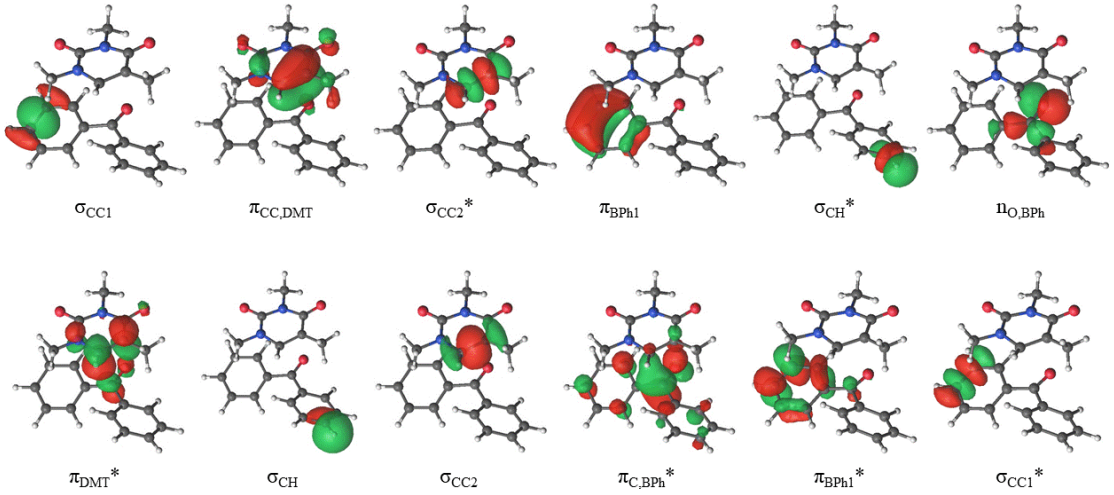

Fig. S5 Natural orbitals of the CASSCF active space of the singlet states at the exciplex structure for HH-1. π_{DMT}^* and $\pi_{C,BP}^*$ can be considered the σ and σ* orbitals of the C-C and C-O bonds that break throughout the process.

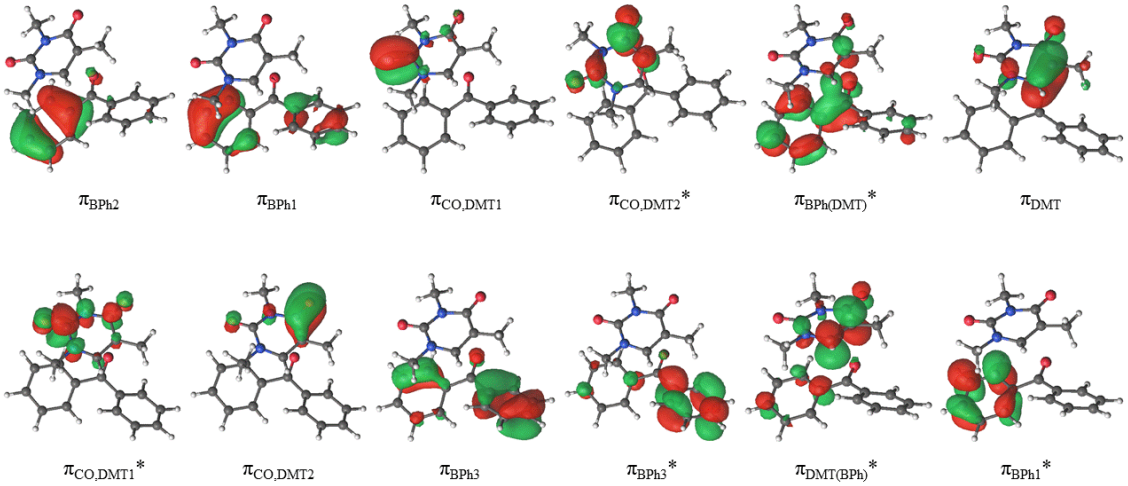

Fig. S6 Natural orbitals of the CASSCF active space of the triplet states at the exciplex structure (^{3}[BP···DMT]*) for HH-1. $\pi_{BP(DMT)}$* and $\pi_{DMT(BP)}$* can be considered the σ and σ* orbitals of the C-C and C-O bonds that break throughout the process.

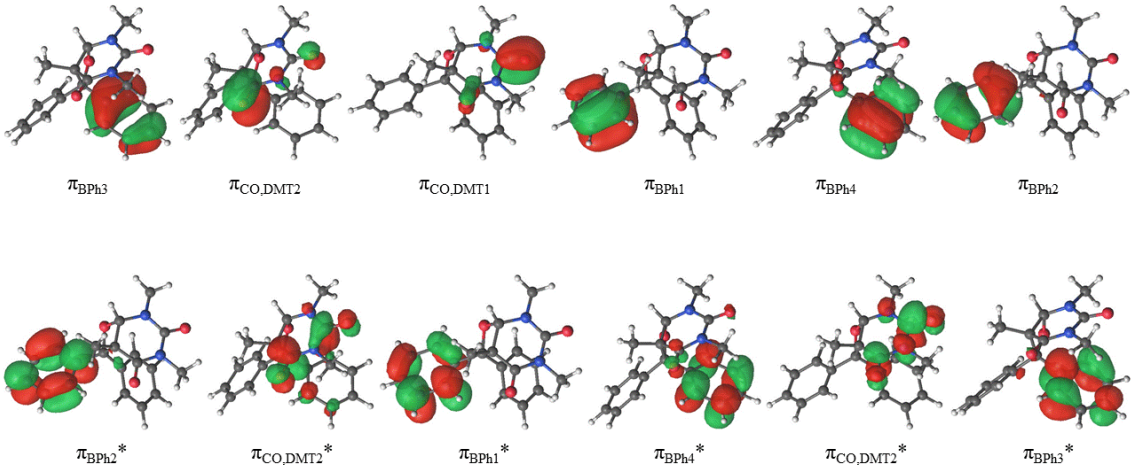

Fig. S7 Natural orbitals of the CASSCF active space of the singlet states at the oxetane structure (OXE) for HT-1.

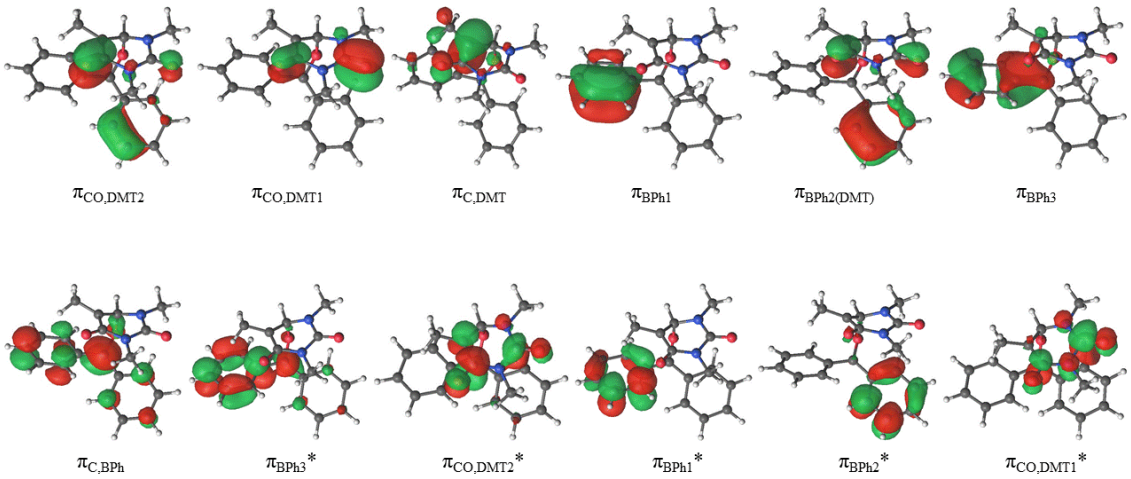

Fig. S8 Natural orbitals of the CASSCF active space of the singlet states of at the diradical structure (^{1}DIR*) for HT-1. $\pi_{C,DMT}$ and $\pi_{C,BP}$ can be considered the σ and σ* orbitals of the C-C bond that breaks throughout the process.

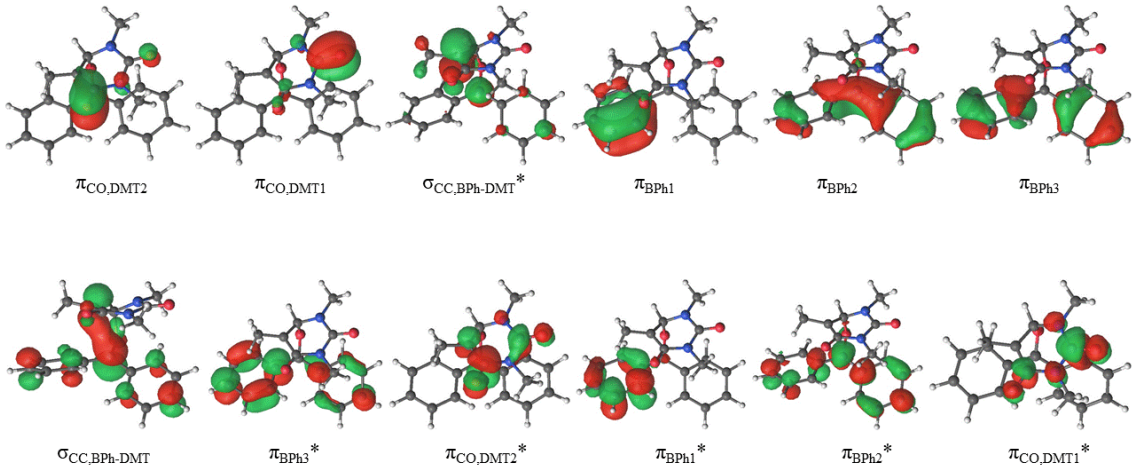

Fig. S9 Natural orbitals of the CASSCF active space of the triplet states at the diradical structure (^{3}DIR*) for HT-1.

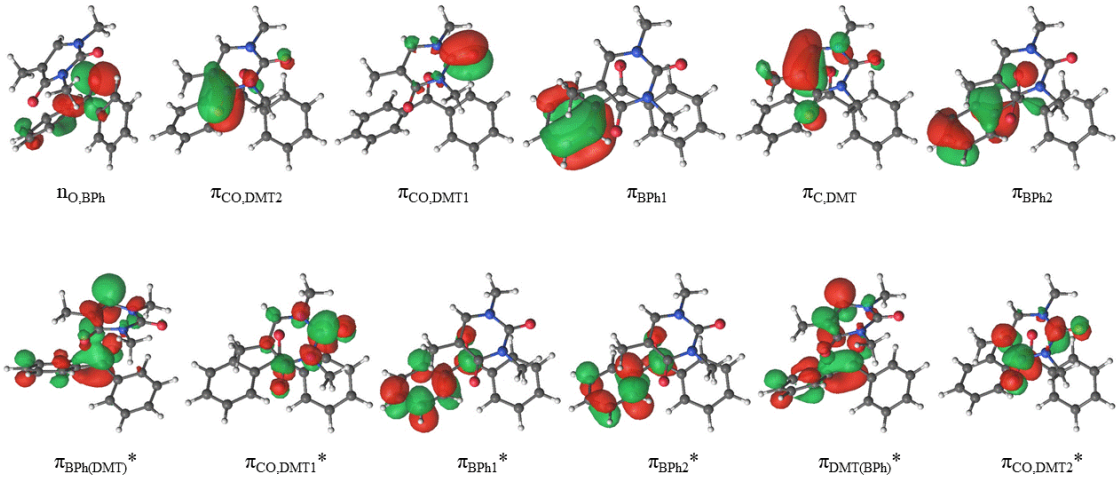

Fig. S10 Natural orbitals of the CASSCF active space of the singlet states at the exciplex structure for HT-1. $\pi_{BP(DMT)}^*$ and $\pi_{DMT(BP)}^*$ can be considered the σ and σ* orbitals of the C-C and C-O bonds that break throughout the process.

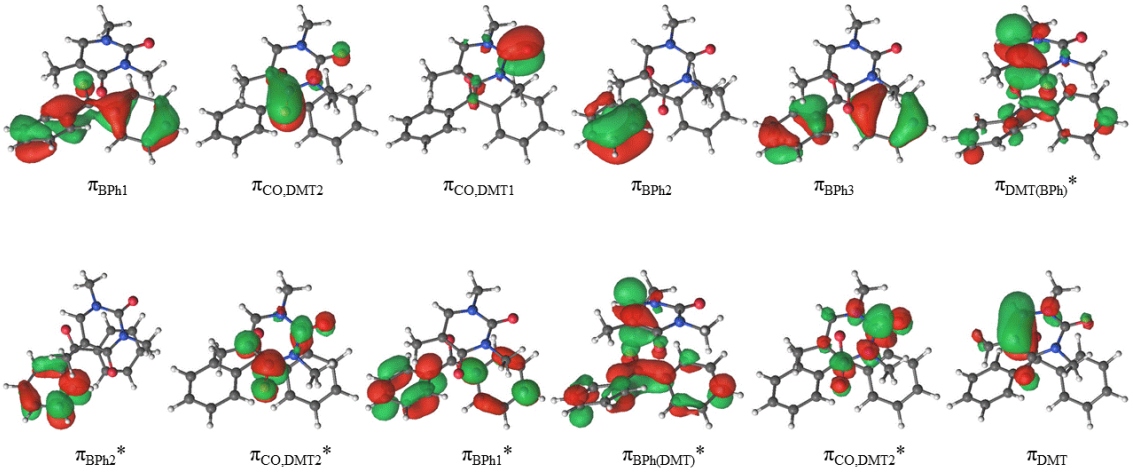

Fig. S11 Natural orbitals of the CASSCF active space of the triplet states at the exciplex structure (^{3}[BP···DMT]*) for HT-1. $\pi_{DMT(BP)}$* and $\pi_{BP(DMT)}$* can be considered the σ and σ* orbitals of the C-C and C-O bonds that break throughout the process.

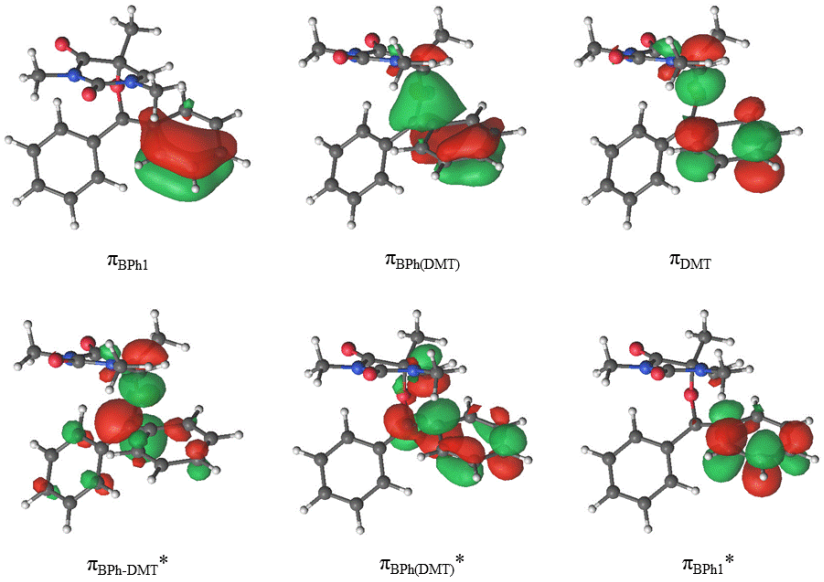

Fig. S12 Natural orbitals of the CASSCF active space at the equilibrium structure of the S_1 state at the diradical region (^{1}DIR*) for HH-1. $\pi_{BP(DMT)}$ and $\pi_{BP(DMT)}$* can be considered the σ and σ* orbitals of the C-C bond that breaks throughout the process.

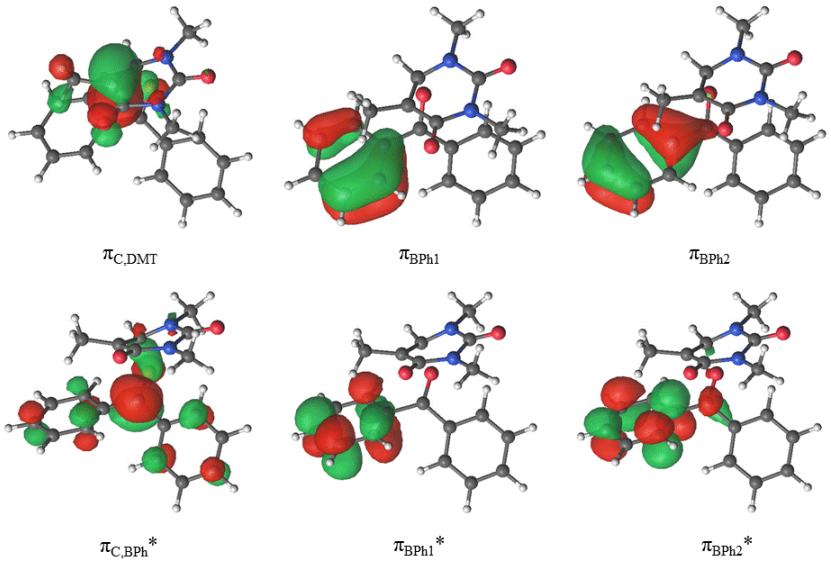

Fig. S13 Natural orbitals of the CASSCF active space at the equilibrium structure of the S_1 state at the diradical region (^{1}DIR*) for HT-1. $\pi_{C,DMT}$ and $\pi_{C,BP}$* can be considered the σ and σ* orbitals of the C-C bond that breaks throughout the process.

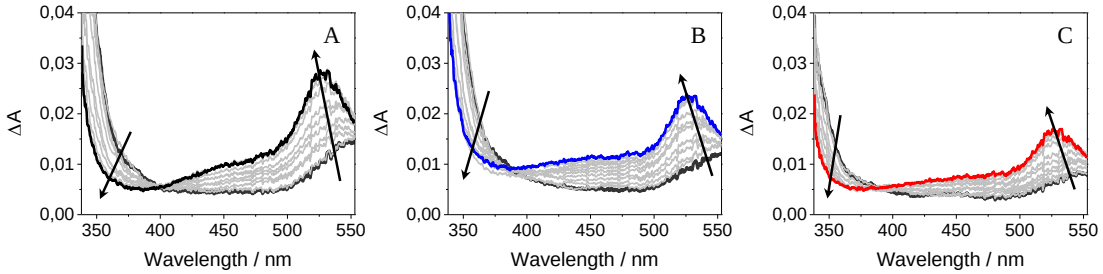

Fig. S14 Femtosecond transient absorption spectra from 0.1 to 40 ps for (A) BP, (B), HH-1 and (C) HT-1 after excitation at 280 nm in MeCN.

References

1. M. J. Frisch, G. W. Trucks, H. B. Schlegel, G. E. Scuseria, M. A. Robb, J. R. Cheeseman, G. Scalmani, V. Barone, B. Mennucci, G. A. Petersson, H. Nakatsuji, M. Caricato, X. Li, H. P. Hratchian, A. F. Izmaylov, J. Bloino, G. Zheng, J. L. Sonnenberg, M. Hada, M. Ehara, K. Toyota, R. Fukuda, J. Hasegawa, M. Ishida, T. Nakajima, Y. Honda, O. Kitao, H. Nakai, T. Vreven, J. J. A. Montgomery, J. E. Peralta, F. Ogliaro, M. Bearpark, J. J. Heyd, E. Brothers, K. N. Kudin, V. N. Staroverov, R. Kobayashi, J. Normand, K. Raghavachari, A. Rendell, J. C. Burant, S. S. Iyengar, J. Tomasi, M. Cossi, N. Rega, J. M. Millam, M. Klene, J. E. Knox, J. B. Cross, V. Bakken, C. Adamo, J. Jaramillo, R. Gomperts, R. E. Stratmann, O. Yazyev, A. J. Austin, R. Cammi, C. Pomelli, J. W. Ochterski, R. L. Martin, K. Morokuma, V. G. Zakrzewski, G. A. Voth, P. Salvador, J. J. Dannenberg, S. Dapprich, A. D. Daniels, Ö. Farkas, J. B. Foresman, J. V. Ortiz, J. Cioslowski and D. J. Fox, Wallingford, CT2013.
2. F. Aquilante, J. Autschbach, R. K. Carlson, L. F. Chibotaru, M. G. Delcey, L. De Vico, I. Fdez. Galván, N. Ferré, L. M. Frutos, L. Gagliardi, M. Garavelli, A. Giussani, C. E. Hoyer, G. Li Manni, H. Lischka, D. Ma, P. Å. Malmqvist, T. Müller, A. Nenov, M. Olivucci, T. B. Pedersen, D. Peng, F. Plasser, B. Pritchard, M. Reiher, I. Rivalta, I. Schapiro, J. Segarra-Martí, M. Stenrup, D. G. Truhlar, L. Ungur, A. Valentini, S. Vancoillie, V. Veryazov, V. P. Vysotskiy, O. Weingart, F. Zapata and R. Lindh, *J. Comput. Chem.*, 2016, **37**, 506-541.
3. N. Forsberg and P.-Å. Malmqvist, *Chem. Phys. Lett.*, 1997, **274**, 196-204.
4. S. Grimme, J. Antony, S. Ehrlich and H. Krieg, *J. Chem. Phys.*, 2010, **132**, 154104.
5. R. M. Parrish, K. C. Thompson and T. J. Martínez, *J. Chem. Theory Comput.*, 2018, **14**, 1737-1753.
6. S. F. Boys and F. Bernardi, *Mol. Phys.*, 2002, **100**, 65-73.
7. D. Roca-Sanjuan, G. Olaso-Gonzalez, I. Gonzalez-Ramirez, L. Serrano-Andres and M. Merchan, *J. Am. Chem. Soc.*, 2008, **130**, 10768-10779.
8. D. C. Sergentu, R. Maurice, R. W. Havenith, R. Broer and D. Roca-Sanjuan, *Phys. Chem. Chem. Phys.*, 2014, **16**, 25393-25403.
9. D. Roca-Sanjuán, G. Olaso-González, I. González-Ramírez, L. Serrano-Andrés and M. Merchán, *J. Am. Chem. Soc.*, 2008, **130**, 10768-10779.
10. L. Serrano-Andrés and M. Merchán, *J. Photochem. Photobiol. C*, 2009, **10**, 21-32.
11. L. Serrano-Andres, M. Merchan and R. Lindh, *J. Chem. Phys.*, 2005, **122**, 104107.